

Stability results for MIMO LTI systems via Scaled Relative Graphs

Eder Baron-Prada, Adolfo Anta, Alberto Padoan and Florian Dörfler

Abstract—This paper proposes a new approach for stability analysis of multi-input, multi-output (MIMO) feedback systems through Scaled Relative Graphs (SRGs). Unlike traditional methods, such as the Generalized Nyquist Criterion (GNC), which relies on a coupled analysis that requires the multiplication of models, our approach enables the evaluation of system stability in a decoupled fashion and provides an intuitive, visual representation of system behavior. Our results provide conditions for certifying the stability of feedback MIMO Linear Time-Invariant (LTI) systems.

I. INTRODUCTION

In control theory, stability is a fundamental property for the reliable operation of feedback systems [1], [2]. Stability influences safety and efficiency across various applications, ranging from industrial automation to power systems [3]. The GNC is a traditional method [1], [4] employed as a critical tool in industrial environments. It provides necessary and sufficient conditions for the stability of feedback systems. However, a significant limitation of this classical approach lies in the inherent coupling: Nyquist diagrams require the multiplication of the transfer functions of all systems in the loop to determine stability, which can be difficult in the case of highly-dimensional systems [1], [5]. In addition, in the case of MIMO systems, the challenges posed by coupled analysis become increasingly pronounced [6]. The interaction of coupled components complicates stability analysis and problem diagnosis, especially in high-order systems where the Nyquist plot may exhibit multiple loops around the origin, which can signal potential instabilities depending on the system.

We propose a new stability result based on the SRG framework to address these limitations. Originally introduced in optimization theory for convergence analysis [7], SRGs have since been applied more broadly, including in the study of stability in nonlinear systems [8], [9]. This approach builds on a homotopy argument, pioneered by Megretski and Rantzer [10] and later widely adopted for stability analysis in diverse systems [9], [11], [12]. While SRGs for LTI systems were first studied by [8], [13], we exploit

the superposition principle to introduce a frequency-wise SRG for LTI systems, significantly reducing conservatism. Our result provides a valuable alternative to the traditional GNC, enabling stability analysis in a decoupled manner. Since the SRG is computed using the system's inputs and outputs, it can be estimated directly from measurements, allowing the technique to be applied in a data-driven manner. This contrasts with traditional methods, such as Lyapunov, eigenvalue analysis, and GNC, which rely on detailed system models [2].

II. PRELIMINARIES

The sets of real and complex numbers are denoted by \mathbb{R} and \mathbb{C} , respectively. The complex conjugate of $z \in \mathbb{C}$ is denoted by z^* . The real and imaginary parts of z are denoted as $\Re(z)$ and $\Im(z)$, respectively. When referring to the angle between two vectors z_1 and z_2 , we use $\angle(z_1, z_2)$. We denote the imaginary unit as j . A matrix A is invertible if there exists a matrix A^{-1} such that $AA^{-1} = A^{-1}A = I$, where I is the identity matrix. Let \mathcal{H} denote a Hilbert space defined over the field F . A square matrix $A : \mathcal{H} \rightarrow \mathcal{H}$ is linear if $A(\alpha x + \beta y) = \alpha A(x) + \beta A(y)$ such that for any $\alpha, \beta \in F$ and $x, y \in \mathcal{H}$. The spectrum of a matrix A consists of all scalar values $\lambda_i \in \mathbb{C}$ such that $(A - \lambda_i I)$ is not invertible.

A. Signal Spaces

We focus on Lebesgue spaces of square-integrable functions \mathcal{L}_2 . Given the time axis, $\mathbb{R}_{\geq 0}$, and a field $F \in \{\mathbb{R}, \mathbb{C}\}$, we define the space $\mathcal{L}_2^n(F)$ by the set of signals $u : \mathbb{R}_{\geq 0} \rightarrow F^n$ and $y : \mathbb{R}_{\geq 0} \rightarrow F^n$ such that the inner product of $u, y \in \mathcal{L}_2^n(F)$ is defined by $\langle u, y \rangle := \int_0^\infty u(t)^* y(t) dt$, and the norm of u is defined by $\|u\| := \sqrt{\langle u, u \rangle} < \infty$. The Fourier transform of $u \in \mathcal{L}_2^n(F)$ is defined as $\hat{u}(j\omega) := \int_0^\infty e^{-j\omega t} u(t) dt$. Moreover, we define the extension of $\mathcal{L}_2^n(F)$ as $\mathcal{L}_{2,e}^n(F) := \{u : \mathbb{R}_{\geq 0} \rightarrow F^n \mid P_T u \in \mathcal{L}_2 \forall T \in \mathbb{R}_{\geq 0}\}$, where $P_T u(t)$ is the truncation operator of the signal $u(t)$ until time T . Note that $\mathcal{L}_2^n \subset \mathcal{L}_{2,e}^n$ [14].

B. Linear Time-Invariant Systems and Transfer Functions

Transfer functions describe the input-output behavior of LTI systems, represented by

$$\dot{x} = Ax + Bu; \quad y = Cx + Du$$

where $x \in \mathbb{R}^n$ is the state vector, $u \in \mathbb{R}^m$ is the input, and $y \in \mathbb{R}^p$ is the output, with the matrices A , B , C , and D of appropriate dimension. By applying the Laplace transform with $x(0) = 0$, we derive the system transfer function as $y(s) = H(s)u(s)$ [1]. An invertible LTI system is defined by a transfer function matrix $H(s)$ that is non-singular for

This work was supported by Innovative Tools for Cyber-Physical Energy Systems (InnoCyPES), under the Marie Skłodowska Curie grant 956433.

Eder Baron is with the Austrian Institute of Technology, 1210 Vienna, Austria, and the Automatic Control Laboratory, ETH Zurich, 8092 Zürich, Switzerland. (e-mail: ebaron@ethz.ch).

Adolfo Anta is with the Austrian Institute of Technology, Vienna 1210, Austria (e-mail: adolfo.anta@ait.ac.at).

Alberto Padoan is with the Department of Electrical & Computer Engineering, University of British Columbia. (e-mail: apadoan@ece.ubc.ca).

Florian Dörfler is with the Automatic Control Laboratory, ETH Zürich, Zürich 8092, Switzerland (e-mail: dorfler@ethz.ch).

We thank Verena Häberle, Linbin Huang, Xiuqiang He, and all members of the IfA group for valuable discussions.

all $s = j\omega$, with $\omega \in \mathbb{R}$, i.e., $\det(H(j\omega)) \neq 0$, ensuring the existence of a unique inverse transfer function $H^{-1}(j\omega)$ satisfying $H(j\omega)H^{-1}(j\omega) = H^{-1}(j\omega)H(j\omega) = I_n$ [4]. This work focuses on the space \mathcal{RH}_∞ of rational, proper, and stable transfer functions, which describe bounded, causal LTI systems. These systems define an input-output gain that measures the ratio of the output size to the input. For \mathcal{L}_2 signals, this gain is equivalent to the H_∞ norm [1], [15]. Moreover, finite incremental gain and asymptotic stability of all input/output trajectories are equivalent for an operator derived from a dynamical system, provided the system is reachable and observable [16]. Finally, the relationship between \mathcal{L}_2 -stability and finite incremental gain does not hold for nonlinear systems where superposition fails.

C. Generalized Nyquist Criterion

The GNC is a fundamental stability method used in control theory to determine if a closed-loop system is stable based on the open-loop frequency response.

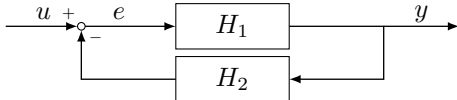


Fig. 1: Feedback interconnection between H_1 and H_2 .

Theorem 1: (GNC) [4], [5] Consider the feedback interconnection in Fig. 1. Assume $H_1(j\omega), H_2(j\omega) \in \mathcal{RH}_\infty^{m \times m}$ and the system interconnection is well-posed. The closed-loop system is exponentially stable if and only if

$$\det(I + H_1(j\omega)H_2(j\omega)) \neq 0, \forall \omega \in \mathbb{R} \quad (1)$$

and the winding number of $(I + H_1(j\omega)H_2(j\omega))$ around the origin is zero.

In Theorem 1 and throughout this paper, the concept of well-posedness is defined in [1, Section 5.2], and the method for calculating the winding number follows the approach outlined in [4, Lemma 4.8]. The winding number is an integer indicating the net number of times a closed curve encircles a point, counting counterclockwise encirclements as +1 and clockwise encirclements as -1. It is computed as the total signed rotations around the point. The GNC comprises two key conditions: the first is a frequency-wise condition, as expressed in (1), while the second involves evaluating the trajectory of (1) over the entire frequency range. A simplified version of the GNC could be formulated as follows.

Theorem 2: (Sufficient GNC) [17] Consider the feedback interconnection in Fig. 1. Assume $H_1(j\omega), H_2(j\omega) \in \mathcal{RH}_\infty^{m \times m}$ and the system interconnection is well-posed. If

$$\det(I + \tau H_1(j\omega)H_2(j\omega)) \neq 0, \forall \tau \in (0, 1], \forall \omega \in \mathbb{R}, \quad (2)$$

then the closed-loop system is exponentially stable.

Theorem 2 provides a sufficient condition for exponential stability. Broadly speaking, it implies that if $\det(I + H_1(j\omega)H_2(j\omega))$ intersects the negative real axis, an encirclement occurs [17]. However, since the theorem does not explicitly track the evolution of the determinant trajectory across the frequency spectrum, it cannot determine if the

winding number of the trajectory around the origin is zero. In scenarios where the models of $H_1(j\omega)$ and $H_2(j\omega)$ are unknown, Theorem 2 serves as the key tool to ensure closed-loop stability. However, similar to classical GNC, Theorem 2 requires the multiplication of the transfer functions for both systems—a condition that can be limiting and prone to numerical inaccuracies. To address this limitation, we instead leverage SRGs, which enable decoupled stability conditions, as demonstrated in the following section.

III. SCALED RELATIVE GRAPHS

SRGs were first introduced in [7], [18] as an analytical tool in optimization theory. We recall its definition and specialize it for linear systems.

A. Scaled Relative Graphs

Consider an operator $A : \mathcal{H} \rightarrow \mathcal{H}$. The SRG of A is defined as [18]

$$\text{SRG}(A) = \left\{ \frac{\|y_2 - y_1\|}{\|u_2 - u_1\|} \exp[\pm j\angle(u_2 - u_1, y_2 - y_1)] \right\}, \quad (3)$$

where $u_1, u_2 \in \mathcal{H}$ are a pair of inputs which outputs are y_1, y_2 , i.e. $y_1 = A(u_1)$ and $y_2 = A(u_2)$. If A is a square matrix, the SRG of A is defined as [13]

$$\text{SRG}(A) = \left\{ \frac{\|y\|}{\|u\|} \exp\left(\pm j \arccos\left(\frac{\Re(\langle y, u \rangle)}{\|y\|\|u\|}\right)\right) \right\}, \quad (4)$$

where $u \in \mathcal{H}, \|u\| = 1$ and $y = Au$, which is equivalent to (3) [18]. The ratio $\frac{\|y\|}{\|u\|}$ represents the amplitude change in the output compared to the input. The term $\frac{\Re(\langle y, u \rangle)}{\|y\|\|u\|}$ indicates the angle between the input and the output [19]. We focus exclusively on square transfer functions, meaning the systems under consideration have equal inputs and outputs ($m = p$), since angular differences between vectors are classically defined for vectors of the same dimension [19]. Such systems are typical in power systems [3] and aircraft/drone systems [20], among others. Note that $\text{SRG}(A)$ is symmetric with respect to the real axis.

B. SRG properties of operators in Hilbert Spaces

We recall three SRG properties: the SRG inverse, the chord property, and the operator class. We define inversion in the complex plane by the Möbius transformation [7]

Property 1 (Inversion of a SRG): If A is an operator, then $\text{SRG}(A^{-1}) = \text{SRG}(A)^{-1} = \{(z^{-1})^* \mid z \in \text{SRG}(A)\}$ [7].

Property 2 (Chord Property): An operator A is said to satisfy the chord property if for every bounded $z \in \text{SRG}(A)$, the line segment $[z, z^*]$, defined as $z_1, z_2 \in \mathbb{C}$ as $[z_1, z_2] := \{\beta z_1 + (1 - \beta)z_2 \mid \beta \in [0, 1]\}$, is in $\text{SRG}(A)$ [7].

We denote by \bar{A} an operator satisfying the chord property such that $\text{SRG}(A) \subseteq \text{SRG}(\bar{A})$. Generally, the SRG does not inherently satisfy the chord property. However, it is always possible to approximate the SRG of any bounded operator to meet the chord property, given that a closed ball in the complex plane can approximate any closed set [19]. Note that the over-approximation is not unique.

Property 3 (Operator Class): Given an operators class \mathcal{A} , the SRG of \mathcal{A} is given by $\text{SRG}(\mathcal{A}) := \bigcup_{A \in \mathcal{A}} \text{SRG}(A)$ [18].

Note that a class does not need any structure. In addition, a class can consist of a single operator.

C. Generalized Feedback Stability Theorem (GFT)

We now recall the GFT in the Theorem 3 originally proposed in [8] and later extended in [9], [21].

Theorem 3: (GFT) Consider the feedback interconnection in Fig. 1 between any pair of operators $A_1 \in \mathcal{A}_1$ and $A_2 \in \mathcal{A}_2$, where $\mathcal{A}_1, \mathcal{A}_2 \in \mathcal{L}_2$ are a class of operators with finite incremental gain. If, for all $\tau \in (0, 1]$,

$$\text{SRG}(\mathcal{A}_1)^{-1} \cap -\tau \text{SRG}(\overline{\mathcal{A}}_2) = \emptyset, \quad (5)$$

then the feedback interconnection maps from \mathcal{L}_2 to \mathcal{L}_2 and is \mathcal{L}_2 stable.

The selection of which SRG to approximate to satisfy the chord property is arbitrary, as discussed in [8]. If finite incremental gain is required, one needs strict separation between the SRGs [9]. The strict separation between $\text{SRG}(\mathcal{A}_1)$ and $\text{SRG}(\mathcal{A}_2)$ is said to hold if the infimum of the absolute distances between any point $a_1 \in \text{SRG}(\mathcal{A}_1)$ and any point $a_2 \in -\text{SRG}(\overline{\mathcal{A}}_2)$, satisfies

$$\inf \{ |a_1 - a_2| \mid a_1 \in \text{SRG}(\mathcal{A}_1), a_2 \in -\text{SRG}(\overline{\mathcal{A}}_2) \} > 0.$$

IV. STABILITY CONDITIONS BASED ON SRGS

In this section, we introduce the frequency-wise version of the SRG for LTI systems and Theorem 4 for evaluating the stability of feedback systems. Finally, we provide conditions under which the Theorem 2 and Theorem 4 are equivalent.

A. SRG of LTI systems

A transfer function $H(j\omega)$ can be regarded as a collection of individual operators, each representing the system response at a specific frequency $\omega \in \mathbb{R}$ [1]. Given the superposition property in linear systems, we can assess stability by examining the system response at each frequency separately rather than analyzing the entire transfer function at once [4]. The SRG allows us to calculate a set of gains and phases for all possible inputs for each operator. By plotting all individual SRGs in a 3D space, we capture the full range of dynamic behaviors of $H(j\omega)$.

The shape of the SRG for LTI systems varies depending on the system dimension. For SISO systems, the SRG at each frequency consists of two symmetrical points about the real axis [13]. In MIMO systems, the SRG forms either two symmetrical curves or two points when $m = 2$. For $m \geq 3$, the SRG can expand into two symmetrical closed regions in the complex plane [13]. Generally, the SRG consists of two disconnected, symmetrical sets across the real axis. However, these sets become connected only if the SRG contains points on the real axis, which occurs when the system has real eigenvalues [22, Proposition 5].

Remark 1 (Chord Property of LTI systems): An LTI system has the chord property if for each $\omega \in [0, \infty)$ and for every $z \in \text{SRG}(H(j\omega))$, the line segment $[z, z^*]$, defined as $z_1, z_2 \in \mathbb{C}$ as $[z_1, z_2] := \{\beta z_1 + (1 - \beta)z_2 \mid \beta \in [0, 1]\}$, is in $\text{SRG}(H(j\omega))$.

B. Decoupled Stability Theorem on LTI systems

This subsection uses the GFT to derive stability conditions based on SRGs for LTI systems. Building on the superposition principle, we present a frequency-wise interpretation of Theorem 3 tailored specifically for LTI systems as follows

Theorem 4: (GFT for LTI systems) Consider the feedback interconnection in Fig. 1. Assume $H_1(j\omega), H_2(j\omega) \in \mathcal{RH}_\infty^{m \times m}$ and the system interconnection is well-posed, either $H_1(j\omega)$ or $H_2(j\omega)$ has the chord property and $H_1(j\omega)$ is invertible. If, $\forall \omega \in [0, \infty)$,

$$\text{SRG}(H_1(j\omega))^{-1} \cap -\tau \text{SRG}(H_2(j\omega)) = \emptyset, \forall \tau \in (0, 1], \quad (6)$$

then the closed-loop system is \mathcal{L}_2 stable.

Proof: The proof can be found in the Appendix A.

Theorem 4 shows that system stability can be evaluated by comparing the SRGs of each system at every frequency $\omega \in [0, \infty)$. Theorem 4 strengthens [8, Theorem 4], which states that the hyperbolic convex hull of the Nyquist plot of $H_1(j\omega)$ is the $\text{SRG}(H_1(j\omega)) \forall \omega \in [0, \infty)$. Prior results [8, Theorem 4] require handling interactions across different frequencies, whereas Theorem 4 removes this constraint. By allowing the system response to be represented as a collection of independent operators at each frequency for both SISO and MIMO systems, Theorem 4 simplifies stability analysis.

C. Equivalence between GFT and GNC

Our main result establishes conditions for H_1 and H_2 under which Theorem 2 and Theorem 4 are equivalent, ensuring \mathcal{L}_2 stability. This analysis focuses exclusively on the interconnection of stable systems, explicitly excluding unstable systems from consideration.

Theorem 5: (Equivalence between GFT and GNC) Consider the feedback interconnection in Fig. 1. Assume $H_1(j\omega), H_2(j\omega) \in \mathcal{RH}_\infty^{m \times m}$ and the system interconnection is well-posed, either $H_1(j\omega)$ or $H_2(j\omega)$ has the chord property and $H_1(j\omega)$ is invertible. Then, the following statements are equivalent:

- 1) $\det(I + \tau H_1(j\omega)H_2(j\omega)) \neq 0 \forall \tau \in (0, 1], \forall \omega \in \mathbb{R}$.
- 2) $\text{SRG}(H_1(j\omega))^{-1} \cap -\tau \text{SRG}(H_2(j\omega)) = \emptyset, \forall \tau \in (0, 1], \forall \omega \in [0, \infty)$.

Proof: The proof can be found in the Appendix B. ■

Theorem 5 provides a frequency-wise sufficient condition for verifying the stability of MIMO LTI systems. By bridging Theorem 2 and Theorem 4, it establishes their equivalence in guaranteeing \mathcal{L}_2 -stability. Importantly, it shows that SRGs can be an alternative to the GNC for stability analysis, providing a complementary tool for studying feedback system stability.

D. Comparison with Nyquist Criterion

The GNC is a classical method for assessing feedback system stability, relying on two key conditions: a frequency-wise condition and a condition encompassing the complete frequency spectrum. While straightforward for SISO systems, its application to MIMO systems introduces significant complexity. Specifically, the analysis requires multiplying the transfer functions $H_1(j\omega)$ and $H_2(j\omega)$ and evaluating their

determinant at every frequency, which becomes computationally challenging for high-dimensional systems. Additionally, interpreting the resulting Nyquist plot can be nontrivial, particularly when many loops appear around the origin, as shown later in Subsection V-C.

In contrast, the SRG-based condition offers a decoupled and computationally streamlined alternative. Instead of combining transfer functions, it evaluates stability by independently analyzing $\text{SRG}(H_1(j\omega))^{-1}$ and $-\text{SRG}(H_2(j\omega))$ at each frequency. This approach not only simplifies MIMO analysis but also provides an intuitive visual representation of system behavior. Moreover, SRGs identify frequency-specific stability margins [9], offering insights for control design. However, this generality comes at a cost as SRGs demand higher computational effort than the GNC, creating a trade-off between analytical power and efficiency. While the Nyquist criterion remains a reliable tool, the SRG method emerges as a flexible and scalable alternative, particularly for complex MIMO systems, as demonstrated numerically in later sections.

V. NUMERICAL EXAMPLES

A. Some illustrative SRGs

To illustrate the differences induced by system dimension, we consider computing the SRGs of the following transfer functions:

$$H_1(s) = \frac{20s + 30}{s^2 + 13s + 30}, \quad (7)$$

$$H_2(s) = \begin{bmatrix} \frac{50s + 2500}{s^2 + 100s + 2501} & \frac{50}{s^2 + 100s + 2501} \\ \frac{30}{s^2 + 100s + 2501} & \frac{30s + 2501}{s^2 + 100s + 2501} \end{bmatrix}, \quad (8)$$

$$H_3(s) = \begin{bmatrix} \frac{s+10}{(s+1)^3(s+2)} & \frac{2}{s+3} & \frac{4}{(s+1)(s+4)} \\ \frac{s+2}{(s+5)^2} & \frac{3}{(s+3)(s+4)} & \frac{3}{s+4} \\ \frac{1}{(s+1)^3} & \frac{3}{s+5} & \frac{2}{(s+3)(s+4)} \end{bmatrix}. \quad (9)$$

Figure 2 presents the SRG representations for all three system cases. For the SISO case, Fig. 2a displays the three-dimensional SRG plot of $H_1(s)$, while Fig. 2b shows its projection onto the complex plane across the frequency range $\omega \in [10^{-5}, 10^5]$ rad/s. Notably, this projection coincides exactly with the Nyquist plot of $H_1(s)$, with the SRG's inherent symmetry capturing both positive and negative frequencies simultaneously. In the $m = 2$ MIMO case, the SRG forms a generalized cylindrical structure, as visible in Fig. 2c. Here, each frequency corresponds to a closed curve, with selected curves highlighted in black to emphasize the continuous, connected nature of the SRG. The most complex case appears when $m = 3$, where Fig. 2d reveals the SRG's full volumetric structure. Black contour lines have been added to this three-dimensional representation to enhance spatial understanding and provide clear visual reference points throughout the SRG's extent.

B. Stability of a MIMO system with $m = 2$

In this section, we aim to prove the efficiency of Theorem

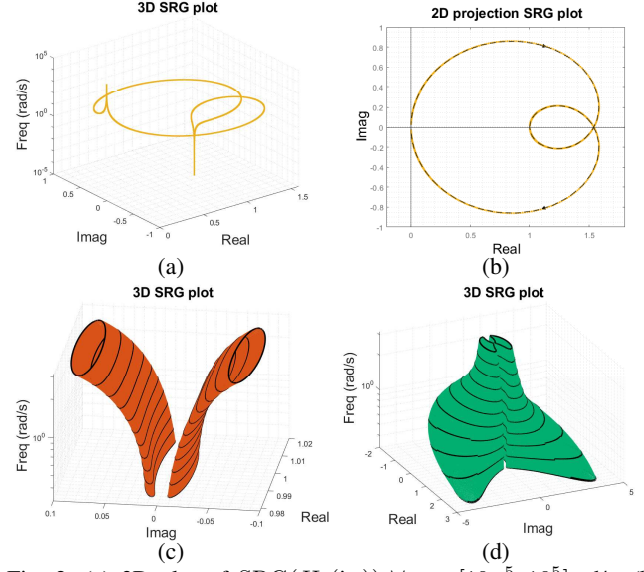


Fig. 2: (a) 3D plot of $\text{SRG}(H_1(j\omega)) \forall \omega \in [10^{-5}, 10^5]$ rad/s. (b) projection of $\text{SRG}(H_1(j\omega))$ in the complex plane in yellow and the Nyquist plot in black dashed line. (c) 3D plot of $\text{SRG}(H_2(j\omega)) \forall \omega \in [0.316, 3.16]$ rad/s. (d) 3D plot of $\text{SRG}(H_3(j\omega)) \forall \omega \in [10^{-1}, 10^1]$ rad/s.

4 and Theorem 2. Consider $H_2(s)$ as (8) and $H_4(s)$ as

$$H_4(s) = \begin{bmatrix} \frac{2s+1}{(s+10)^3} & \frac{s+12}{(s+1)^2} \\ \frac{5s+10}{(s+15)^3} & \frac{s+22}{(s+6)(s+10)^2} \end{bmatrix}. \quad (10)$$

Fig. 3 presents $-\tau \text{SRG}(H_4(j\omega))$ with $\tau = 1$ and $\text{SRG}(H_2^{-1}(j\omega))$. Fig. 3a provides a 3D plot of the SRG for both operators, though this plot alone does not yield conclusive insights. To facilitate clearer interpretation, we include two projections onto the complex plane for two different frequency ranges in Fig. 3b and Fig. 3c. As shown in Figures 3a, 3b, and 3c, $-\text{SRG}(H_4(j\omega))$ exhibits varying area in the complex plane across the frequency spectrum, expanding to a larger region at low frequencies ($\omega < 1$ rad/s) and contracting at higher frequencies ($\omega > 1$ rad/s).

Conversely, $\text{SRG}(H_2^{-1}(j\omega))$ exhibits an opposite pattern to $-\text{SRG}(H_4(j\omega))$. Specifically, Figure 3b shows the low-frequency behavior ($\omega < 1$ rad/s), where $\text{SRG}(H_2^{-1}(j\omega))$ occupies a smaller region. However, at higher frequencies ($\omega > 1$ rad/s), $\text{SRG}(H_2^{-1}(j\omega))$ expands to cover a broader area, as illustrated in Figure 3c. Furthermore, when Theorem 4 is assessed it shows that the system is stable, given that $-\tau \text{SRG}(H_4(j\omega)) \forall \tau \in (0, 1]$ does not intersect $\text{SRG}(H_2^{-1}(j\omega))$ at any frequency. The Nyquist plot shown in Fig. 3d can also guarantee the \mathcal{L}_2 stability.

C. Stability of a high order MIMO system with $m = 3$

Consider a square system, $H(j\omega)$, with $m = 3$ of order 50, i.e., with 50 stable poles, generated by the Matlab command `rss(50, 3, 3)`, with no unstable zeros¹. Furthermore, con-

¹The system under analysis can be found at <https://github.com/eder-baron/SRG-ECC-2025>

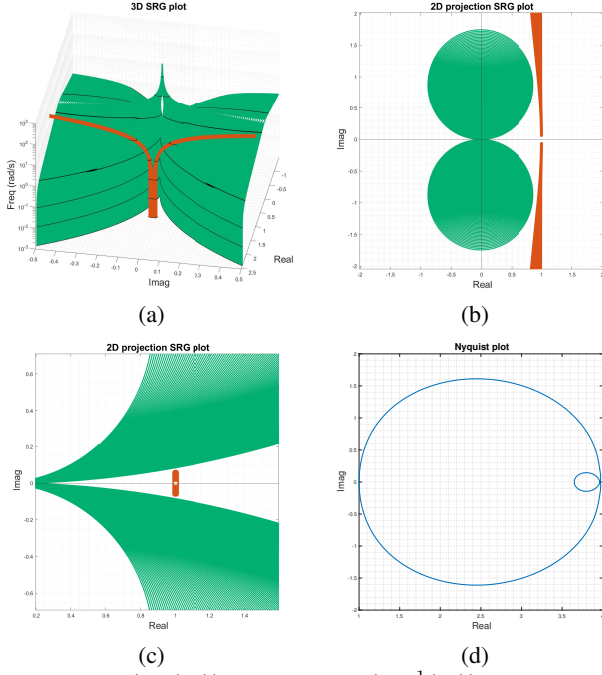


Fig. 3: $-\text{SRG}(H_4(j\omega))$ in green, $\text{SRG}(H_2^{-1}(j\omega))$ in orange $\forall \omega \in [10^{-3}, 10^3]$ rad/s. (a) SRGs 3D visualization. (b) 2D projection of the SRGs in the complex plane for $\omega \in [10^{-3}, 1]$ rad/s. (c) 2D projection of the SRGs in the complex plane for $\omega \in [1, 10^3]$ rad/s. (d) Nyquist plot using $\det(I + H_4(j\omega)H_2(j\omega))$.

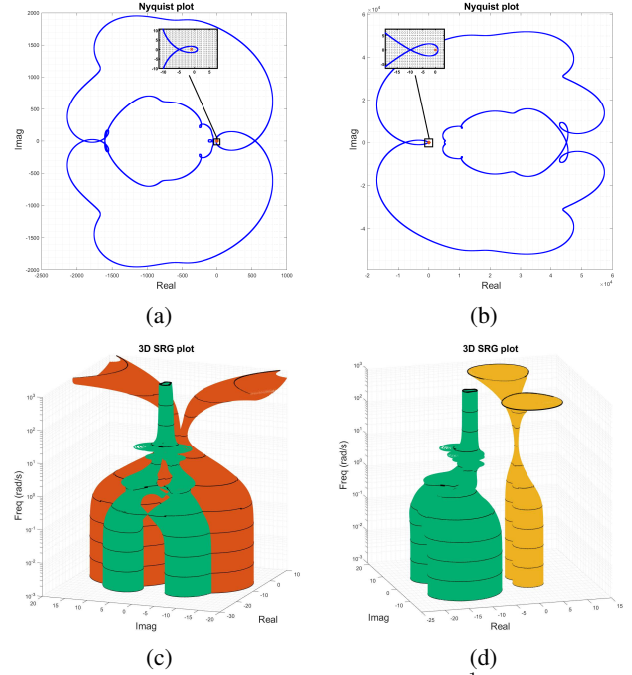


Fig. 4: $\text{SRG}(H(j\omega))$ in green, $-\text{SRG}(H_5^{-1}(j\omega))$ in orange and $-\text{SRG}(H_6^{-1}(j\omega))$ in yellow $\forall \omega \in [10^{-3}, 10^3]$ rad/s. (a) Nyquist plot of $\det(I + H(j\omega)H_5(j\omega))$ (b) Nyquist plot of $\det(I + H(j\omega)H_6(j\omega))$ (c) 3D plot of the $\text{SRG}(H(j\omega))$ and $-\text{SRG}(H_5^{-1}(j\omega))$ (d) 3D plot of the $\text{SRG}(H(j\omega))$ and $-\text{SRG}(H_6^{-1}(j\omega))$.

sider $H_5(j\omega)$ and $H_6(j\omega)$ as (11) and (12).

$$H_5(j\omega) = \begin{bmatrix} \frac{33(s+1)}{(s+\frac{143}{10})^2} & \frac{18(s+14)}{5(s+15)^2} & \frac{21(s+\frac{23}{10})}{5(s+15)^2} \\ \frac{36(s+2)}{(s+14)(s+55)} & \frac{39(s+13)}{(s+15)(s+\frac{27}{2})} & \frac{30(s+2)}{(s+15)^2} \\ \frac{30(s+\frac{3}{2})}{(s+7)^2} & \frac{18(s+\frac{9}{2})}{5(s+4)(s+\frac{7}{2})} & \frac{39(s+3)}{(s+15)^2} \end{bmatrix}, \quad (11)$$

$$H_6(j\omega) = - \begin{bmatrix} \frac{88(s+1)}{(s+\frac{143}{10})^2} & \frac{48(s+14)}{5(s+15)^2} & \frac{56(s+\frac{23}{10})}{5(s+15)^2} \\ \frac{96(s+2)}{(s+14)(s+55)} & \frac{104(s+13)}{(s+15)(s+\frac{27}{2})} & \frac{80(s+2)}{(s+15)^2} \\ \frac{80(s+\frac{3}{2})}{(s+7)^2} & \frac{48(s+\frac{9}{2})}{5(s+24)(s+\frac{27}{2})} & \frac{104(s+3)}{(s+15)^2} \end{bmatrix}. \quad (12)$$

In this example, the feedback loop of $H(j\omega)$ and $H_5(j\omega)$ is unstable, while the feedback loop of $H(j\omega)$ and $H_6(j\omega)$ is stable. Figs 4a and 4c show the Nyquist and SRG plots of the feedback loop between $H(j\omega)$ and $H_5(j\omega)$. Furthermore, we depict the same plots for the feedback loop between $H(j\omega)$ and $H_6(j\omega)$ in Figs 4b and 4d. Figs. 4a and 4b show two Nyquist plots for MIMO systems using the GNC. It is possible to observe that the Nyquist plot does multiple loops around the origin in both plots, making it particularly difficult to use Theorem 1 to certify the stability of both closed-loop systems. When we examine Fig. 4c, it is possible to observe intersections between both SRGs along the entire frequency spectrum, where we can conclude that the closed loop system with $H_5(j\omega)$ is unstable.

As in Fig. 4a, the Nyquist plot in Fig. 4b shows multiple loops around the origin, and thus it fails to satisfy the conditions of Theorem 2 for ensuring stability, as the Nyquist plot exhibits crossings with the negative real axis. Addi-

tionally, Fig. 4d illustrates the 3D plot of $-\text{SRG}(H(j\omega))$ and $\text{SRG}(H_5^{-1}(j\omega))$. When scaling $-\tau \text{SRG}(H(j\omega))$ for all $\tau \in (0, 1]$, intersections between the SRGs occur, showing that Theorem 4 is unsuitable in this case. Despite this, since Fig. 4b confirms that the winding number around the origin is zero, the stability of the feedback loop can still be guaranteed by Theorem 1, given that (1) is met across the entire frequency spectrum. The SRGs maintain complete separation across the entire frequency spectrum in the stable feedback system (Fig. 4d). This empirical evidence suggests that SRG separation with $\tau = 1$ might be sufficient for guaranteeing \mathcal{L}_2 stability. Theoretical verification of SRG separation as necessary and sufficient condition for stability remains an important open question.

VI. CONCLUSIONS

We derive an alternative to the frequency-wise version of the GNC using SRGs, benefiting from a decoupled approach that simplifies stability analysis. This method provides deeper insights into the system's dynamic behavior across frequencies. Future work will aim to extend this approach to more general systems.

REFERENCES

- [1] K. Zhou and J. C. Doyle, *Essentials of robust control*. Prentice hall Upper Saddle River, NJ, 1998, vol. 104.
- [2] H. Khalil, *Nonlinear Systems*. Prentice Hall, 2002.
- [3] L. Huang, D. Wang, X. Wang, H. Xin, P. Ju, K. H. Johansson, and F. Dörfler, "Gain and phase: Decentralized stability conditions for power electronics-dominated power systems," *IEEE Transactions on Power Systems*, 2024.

- [4] S. Skogestad and I. Postlethwaite, *Multivariable feedback control: analysis and design*. John Wiley & sons, 2005.
- [5] C. Desoer and Y.-T. Wang, "On the generalized Nyquist stability criterion," *IEEE Transactions on Automatic Control*, 1980.
- [6] D. Wang, W. Chen, and L. Qiu, "The first five years of a phase theory for complex systems and networks," *IEEE/CAA Journal of Automatica Sinica*, vol. 11, no. 8, pp. 1728–1743, 2024.
- [7] E. Ryu and W. Yin, *Large-Scale Convex Optimization: Algorithms & Analyses via Monotone Operators*. Cambridge Univ. Press, 2022.
- [8] T. Chaffey, F. Forni, and R. Sepulchre, "Graphical nonlinear system analysis," *IEEE Transactions on Automatic Control*, 2023.
- [9] T. Chaffey, A. Kharitenko, F. Forni, and R. Sepulchre, "A homotopy theorem for incremental stability," *arXiv preprint:2412.01580*, 2024.
- [10] A. Megretski and A. Rantzer, "System analysis via integral quadratic constraints," *IEEE Transactions on Automatic Control*, 1997.
- [11] J. Grönqvist and A. Rantzer, "Integral quadratic constraints for neural networks," in *2022 European Control Conference (ECC)*, 2022.
- [12] U. Jonsson, C.-Y. Kao, and A. Megretski, "A semi-infinite optimization problem in harmonic analysis of uncertain systems," in *American Control Conference (ACC)*, 2001.
- [13] R. Pates, "The scaled relative graph of a linear operator," *arXiv preprint:2106.05650*, 2021.
- [14] A. Van der Schaft, *L2-gain and passivity techniques in nonlinear control*. Springer, 2000.
- [15] W. Chen, D. Wang, S. Z. Khong, and L. Qiu, "A phase theory of MIMO LTI systems," *arXiv preprint:2105.03630*, 2021.
- [16] V. Fromion, S. Monaco, and D. Normand-Cyrot, "A link between input-output stability and lyapunov stability," *Systems & Control Letters*, 1996.
- [17] W. M. Griggs, S. S. K. Sajja, B. D. Anderson, and R. N. Shorten, "On interconnections of "mixed" systems using classical stability theory," *Systems & Control Letters*, 2012.
- [18] E. K. Ryu, R. Hannah, and W. Yin, "Scaled relative graphs: nonexpansive operators via 2d euclidean geometry," *Mathematical Programming*, vol. 194, no. 1–2, p. 569–619, jun 2021.
- [19] R. S. Millman and G. D. Parker, *Geometry: a metric approach with models*. Springer Science & Business Media, 1993.
- [20] Y. Marani, K. Telegenov, E. Feron, and M.-T. L. Kirati, "Drone reference tracking in a non-inertial frame: control, design and experiment," in *2022 IEEE/AIAA 41st Digital Avionics Systems Conference*, 2022.
- [21] C. Chen and R. Sepulchre, "On the scaled relative graph separation for feedback incremental stability," in *Benelux Meeting 2024*, 2024.
- [22] R. Hannah and W. Yin, "Scaled relative graph," *UCLA CAM report*, 2016.

APPENDIX

A. Proof Theorem 4

Since $H_1(j\omega)$ and $H_2(j\omega)$ are transfer functions, we can analyze their stability at each frequency by applying the superposition principle [1], [2]. Hence, we consider the following operator classes for each $\omega \in [0, \infty)$

$$\mathcal{A}_{1,\omega} := H_1(j\omega), \mathcal{A}_{2,\omega} := H_2(j\omega).$$

We apply Theorem 3 to each pair $\mathcal{A}_{1,\omega}$ and $\mathcal{A}_{2,\omega}$. Since $H_1(j\omega)$ and $H_2(j\omega)$ belong to $\mathcal{RH}_\infty^{m \times m}$, the conditions for applying the theorem are satisfied (finite incremental gain [1, Section 4.2]). Using (5), we obtain

$$\text{SRG}(\mathcal{A}_{1,\omega})^{-1} \cap -\tau \text{SRG}(\overline{\mathcal{A}}_{2,\omega}) \neq \emptyset, \quad (13)$$

for each $\omega \in [0, \infty)$. Since $H_1(j\omega)$ or $H_2(j\omega)$ has the chord property for each $\omega \in [0, \infty)$, (13) is equivalent to

$$\text{SRG}(H_1(j\omega))^{-1} \cap -\tau \text{SRG}(H_2(j\omega)) = \emptyset, \quad (14)$$

for each $\omega \in [0, \infty)$. \blacksquare

B. Proof Theorem 5

Now we prove 1) \Rightarrow 2). We recall the Minkowski sum of two sets A and B as $A + B = \{a + b \mid a \in A, b \in B\}$. In addition, we recall the frequency-wise version of the GNC as

$$\det(I + \tau H_1(j\omega)H_2(j\omega)) \neq 0, \quad \forall \tau \in (0, 1].$$

Since $H_1(j\omega)$ is invertible, a multiplication of the GNC with $\det(H_1^{-1}(j\omega))$ does not modify the original condition, i.e.,

$$\det(H_1^{-1}(j\omega)) \det(I_n + \tau H_1(j\omega)H_2(j\omega)) \neq 0. \quad (15)$$

We use the determinant properties of the Schur complement to represent (15) as

$$\det \left(\begin{bmatrix} H_1^{-1}(j\omega) & -\tau H_2(j\omega) \\ I_n & I_n \end{bmatrix} \right) \neq 0,$$

or equivalently as $\det(I_n) \det(H_1^{-1}(j\omega) + \tau H_2(j\omega)) \neq 0$. Since the determinant of a matrix is the product of its eigenvalues, we have equivalently

$$\prod_{i=1}^n \lambda_i(H_1^{-1}(j\omega) + \tau H_2(j\omega)) \neq 0. \quad (16)$$

Equation (16) holds if $\lambda_i(H_1^{-1}(j\omega) + \tau H_2(j\omega)) \neq 0 \quad \forall i$. The spectrum lies within the SRG, i.e., $\text{SRG}(A) \supseteq \lambda(A)$ [13, Thm 1]. Additionally, $0 \in \text{SRG}(A)$ if and only if any $\lambda_i(A) = 0$. Hence, (16) implies

$$0 \notin \text{SRG}(H_1^{-1}(j\omega) + \tau H_2(j\omega)), \quad (17)$$

Since $H_1(j\omega)$ or $H_2(j\omega)$ have the chord property [18, Thm 6], it follows that

$$\text{SRG}(H_1^{-1}(j\omega) + \tau H_2(j\omega)) = \text{SRG}(H_1^{-1}(j\omega)) + \text{SRG}(\tau H_2(j\omega)).$$

Thus, (17) can be written as

$$0 \notin \text{SRG}(H_1^{-1}(j\omega)) + \text{SRG}(\tau H_2(j\omega)), \quad (18)$$

which means that for each ω , there should not be any intersection between $\text{SRG}(H_1^{-1}(j\omega))$ and $-\text{SRG}(\tau H_2(j\omega))$. We can rewrite (18) as

$$\text{SRG}(H_1(j\omega))^{-1} \cap -\tau \text{SRG}(H_2(j\omega)) = \emptyset, \quad (19)$$

which is the GFT for LTI systems in (6). Therefore, we can conclude that $\det(I + \tau H_1(j\omega)H_2(j\omega)) \neq 0 \quad \forall \tau \in (0, 1]$ is equivalent to (6) for LTI MIMO systems $\in \mathcal{RH}_\infty$ for each $\omega \in [0, \infty)$.

The implication 2) \Rightarrow 1) can be established by reversing the steps used in the proof of 1) \Rightarrow 2). \blacksquare